MOLECULAR AND CELLULAR BIOLOGY, Nov. 2001, p. 7707–7713 Vol. 21, No. 22
0270-7306/01/$04.00+0 DOI: 10.1128/MCB.21.22.7707–7713.2001

Targeted Disruption of the Myocilin Gene (*Myoc*) Suggests that Human Glaucoma-Causing Mutations Are Gain of Function

BYONG SU KIM,[1] OLGA V. SAVINOVA,[2] MARK V. REEDY,[1] JANICE MARTIN,[2] YI LUN,[1] LIN GAN,[1,3] RICHARD S. SMITH,[2,4] STANISLAV I. TOMAREV,[5] SIMON W. M. JOHN,[2,4,6] AND RANDY L. JOHNSON[1,7]*

Department of Biochemistry and Molecular Biology[1] and Program in Genes and Development,[7] University of Texas, M. D. Anderson Cancer Center, Houston, Texas 77030; The Jackson Laboratory[2] and The Howard Hughes Medical Institute,[4] Bar Harbor, Maine 04609; Laboratory of Molecular and Developmental Biology, National Eye Institute, National Institutes of Health, Bethesda, Maryland 20892[5]; Department of Ophthalmology Tufts University School of Medicine, Boston, Massachusetts 02111[6]; and Center for Aging and Developmental Biology, University of Rochester, Rochester, New York 14642[3]

Received 4 April 2001/Returned for modification 10 July 2001/Accepted 6 August 2001

Glaucoma is a heterogeneous eye disease and a major cause of blindness worldwide. Recently, primary open angle glaucoma (POAG)-associated mutations have been found in the trabecular meshwork inducible glucocorticoid response gene (*TIGR*), also known as the myocilin gene (*MYOC*), at the *GLC1A* locus on chromosome 1q21-q31. These mutations occurred in a subset of patients with juvenile- and adult-onset POAG and exhibited autosomal dominant inheritance. Ocular expression and its involvement in POAG suggest that *TIGR*/*MYOC* may have a role(s) in regulating intraocular pressure (IOP). Here, we report the generation and analysis of mice heterozygous and homozygous for a targeted null mutation in *Myoc*. Our study shows that *Myoc* mutant mice are both viable and fertile. Our in vivo findings further demonstrate that *Myoc* is not required for normal IOP or normal ocular morphology. The lack of a discernable phenotype in both *Myoc*-heterozygous and *Myoc*-null mice suggests that haploinsufficiency is not a critical mechanism for POAG in individuals with mutations in *MYOC*. Instead, disease-causing mutations in humans likely act by gain of function.

Glaucoma is a heterogeneous eye disease in which affected individuals experience gradual loss of vision due to ocular neuropathies involving retinal ganglion cell death and the optic nerve layer (25). It is a major cause of blindness worldwide affecting an estimated 67 million people (24). Although glaucoma can be treated successfully if detected early, the disease is largely asymptomatic in its initial phase, making early detection difficult. Most affected individuals first experience mild peripheral visual field loss, followed by more extensive peripheral and central visual field deficiencies, which are irreversible. Currently, a limited number of medical interventions are available for treating glaucoma following early detection.

The anterior chamber of the eye is filled with aqueous humor, a clear fluid whose production and outflow are regulated by the ciliary body and the trabecular meshwork, respectively. The trabecular meshwork is a small tissue located at the iridocorneal angle in the corneoscleral transition zone of the anterior chamber. In some cases of glaucoma, structural abnormalities associated with the trabecular meshwork are believed to impede drainage of aqueous humor and consequently lead to an elevated intraocular pressure (IOP) (6, 19, 25). Although not all cases of glaucoma involve abnormally high levels of IOP, an IOP elevated above the normal level is accepted as a considerable risk factor in primary open angle glaucoma (POAG) (6). How elevated IOP contributes to visual field loss, however, is not clearly understood.

A number of loci are currently known in humans that cosegregate with different types of glaucoma. For example, *LMX1B*, *FOXC1*, *PITX2*, and *PAX6* encode transcription factors necessary for normal development of the eye and the anterior segment, and mutations in these genes were found to cosegregate with different types of developmental glaucoma (7, 8, 14, 16, 22, 35). Recently, mutations of the trabecular meshwork inducible glucocorticoid response gene (*TIGR*), now widely referred to as the myocilin gene (*MYOC*), were identified at the *GLC1A* locus on chromosome 1q21-q31 and shown to occur in a subset of families with a high incidence of juvenile- and adult-onset POAG (30). Additional diseases causing *TIGR*/*MYOC* mutations have subsequently been observed in other studies (2, 28, 29, 31).

MYOC is expressed in the eye, including the retina and the structures involved in aqueous humor regulation such as the trabecular meshwork and ciliary body (13, 15, 33). In the mouse, *Myoc* mRNA expression is also detected in the skeletal muscle, heart, brain, and testis, suggesting a role(s) in these tissues (1, 32, 34). MYOC has two domains, one with homology to nonmuscle myosin of *Dictyostelium discoideum* and the other with homology to olfactomedin protein, an extracellular matrix protein first described in the olfactory epithelium of bullfrog (36). The homology to olfactomedin protein and the presence of a signal peptide at its N terminus suggest that MYOC is an extracellular protein (21). In addition, recombinant MYOC is present in the conditioned medium of tissue culture cells (23). However, MYOC has also been detected

* Corresponding author. Mailing address: Box 117, Department of Biochemistry and Molecular Biology, University of Texas, M. D. Anderson Cancer Center, Houston, TX 77030. Phone: (713) 792-2551. Fax: (713) 791-9478. E-mail: rjohnson@odin.mdacc.tmc.edu.

intracellularly in the trabecular cells and cilia of photoreceptor cells (13, 15). Despite a series of molecular characterizations, no specific function of MYOC has yet been described.

To address the requirements for *Myoc* in normal ocular function, we generated a null mutation at the *Myoc* locus by gene targeting in mice. Because glaucoma is often age related, we have maintained our *Myoc* mutant mouse colonies for almost 2 years. Mice heterozygous (+/−) and homozygous (−/−) for the null mutation in *Myoc* are both viable and fertile. We also measured the IOPs of mutant mice and found that IOP was normal even in aged mice. Additionally, we found no significant phenotypic alterations within mutant ocular tissues when examined at the light and ultrastructural microscopic levels. In conclusion, our in vivo findingss demonstrate that *Myoc* is not required for normal development, fertility, or viability in mice. Moreover, we found that reduction of gene dosage or elimination of the *Myoc* gene product is not sufficient to cause any discernable abnormality in the mouse eye. The lack of ocular phenotypes in both +/− and −/− mice also suggests that haploinsufficiency is not a critical mechanism for POAG in individuals with mutations in *MYOC* and that disease-causing mutations in humans are likely gain of function.

MATERIALS AND METHODS

In situ hybridization and *lacZ* staining. Section in situ hybridization with ^{35}S-labeled cRNA probes was performed as described (3). An *Nco*I-*Xba*I *Myoc* genomic DNA fragment containing the 5′ untranslated region (5′-UTR) and the entire coding region of exon 1 was subcloned into the pBSK+ plasmid. The plasmid was then digested with *Xho*I and *Bam*HI for sense-T3 and antisense-T7 riboprobe synthesis, respectively. For *lacZ* staining, cryostat sections of mutant eyes were postfixed in 2% paraformaldehyde, 0.2% glutaldehyde, and 0.02% NP-40 in phosphate-buffered saline (PBS). Following PBS washes, the staining reaction mixture was developed in 25 mg of X-gal (S-bromo-4-chloro-3-indoyl-β-D-galactopyranoside) per ml of dimethyl sulfoxide at 37°C. Counterstaining was performed with 0.1% eosin.

Targeting constructs and generation of *Myoc*-null mice. A 129 SvEv (129) mouse genomic library was screened with a probe (0.4 kb) from the 5′ region of *Myoc*, yielding several hybridizing clones. The targeting vector was made using a 1.7-kb *Eco*RV/*Pvu*II fragment as the 5′ arm of homology and a 2.1-kb *Xba*I fragment as the 3′ arm of homology. Homologous recombination results in deletion of a portion of the 5′-UTR, the entire coding region of exon 1, and approximately 180 bp in the 5′ region of intron 1 (Fig. 1A). The deleted genomic fragment was replaced with an *IRES-lacZ-polyA*-floxed *pgk-neomycin* cassette (M. Wakamiya, personal communication). An Mc1tk cassette was placed outside the 5′ arm of homology for negative selection. The plasmid was linearized at a unique *Not*I site and electroporated into the mouse AB1 embryonic stem (ES) cells. The targeted ES cells were then injected into albino C57BL/6 (B6) blastocysts. Cell culture, generation of chimeric mice, and germ line transmission were performed as described (5). Genotyping of ES cells was performed by Southern hybridization. Subsequent genotyping of animals was performed either by Southern hybridization or by PCR with genomic DNA isolated from the tails of 1- to 2-week-old mice. For Southern blot analysis, genomic DNA (10 μg) was digested with *Xba*I or *Hin*dIII for hybridization with 5′ or 3′ probes, respectively. PCR primers specific for the wild-type allele were my-s5 (5′-CCTCACCCAGC CTCCACACT-3′) and mm1r2-r (5′-GTGAAGGTGTATTGGCATCG-3′), and primers specific for the targeted allele were lacz1 (5′-GCATCGAGCTGGGTA ATAAGGGTTGGCAAT-3′) and lacz2 (5′-GACACCAGACCAACTGGTAA TGGTAGCGAC-3′) (Fig. 1B). The PCR was performed for 30 cycles by denaturing at 94°C for 45 s, annealing at 59°C for 45 s, and elongation at 72°C for 60 s. For RT reverse transcription (RT)-PCR, eyes from 1-month-old animals were homogenized in 1 ml of TRIzol Reagent (Gibco BRL). The procedures for RNA isolation and first-strand cDNA synthesis using SuperScript II were all performed as recommended by the manufacturer. RT-PCR oligonucleotides used were as follows: forward primer, mm1f2 (5′-CGATGCCAATACACCTTCAC-3′) for *Myoc* exon 1; forward primer, e2f1 (5′-GGTTCCTGCTTCCCAAATCT-3′) for *Myoc* exon 2; reverse primer, mm3r1 (5′-CTCTCCAGGGGGTTGTAG TC-3′) for *Myoc* exon 3 (Fig. 1B). For an RT-PCR positive control, a set of oligonucleotides specific for exon 6 (pf1; 5′-AGGGCAATCGGAGGGAGTA-3′) and exon 7 (pr2; 5′-TGTGGTGGGCTGTGGGATTG-3′) of mouse *Pax6* was used. The PCR was performed for 30 cycles by denaturing at 94°C for 30 s, annealing at 61°C for 45 s, and elongation at 72°C for 90 s.

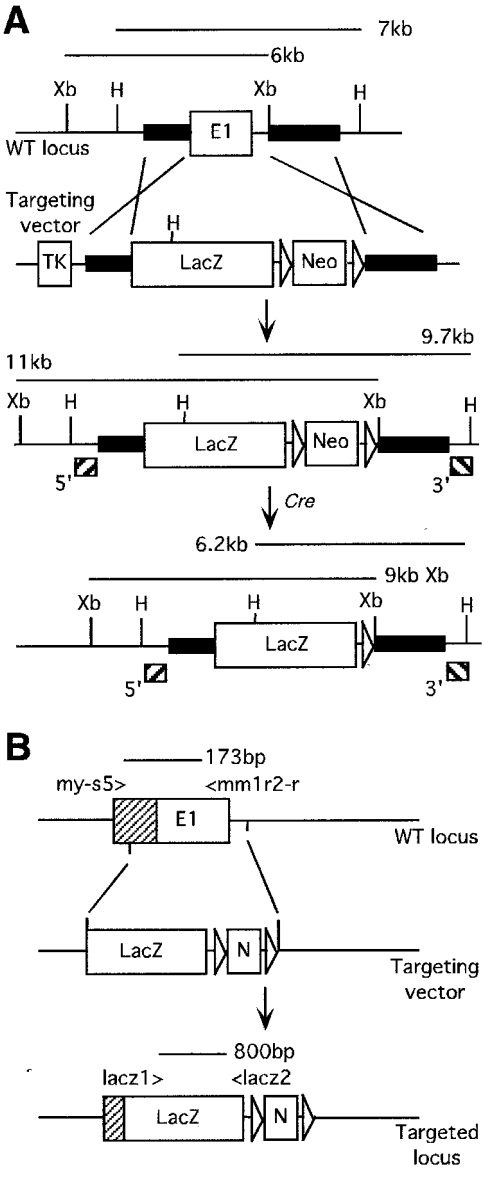

FIG. 1. Generation of *Myoc*-null mice. (A) Schematic representation of a portion of the mouse *Myoc* locus and targeting strategy. The targeted disruption results in 11-kb *Xba*I and 9.7-kb *Hin*dIII fragments when hybridized with 5′ and 3′ Southern probes, respectively. The *neo* cassette was removed from the targeted locus through *Cre*-mediated recombination, which is indicated by hybridizations of 9-kb *Xba*I and 6.2-kb *Hin*dIII fragments. (B) PCR-based analysis of the targeting event. A pair of PCR primers, my-s5 and mm1r2-r, amplify a 173-bp fragment for the wild-type allele. lacz1 and lacz2 PCR primers amplify an internal fragment of approximately 800 bp from *IRES-lacZ-pA*, for the targeted locus. E1, exon 1; shaded box, 5′-UTR; Xb, *Xba*I; H, *Hin*dIII; TK, Mc1tk; LacZ, *IRES-lacZ-pA*; Neo, ploxed *neo*; E, *Eco*RI; P, *Pvu*II.

Western blot analysis. Polyclonal rabbit antiserum was raised against a glutathione *S*-transferase fusion protein containing amino acids 100 to 187 of the mouse MYOC, encoded within exon 1. Equal amounts of total eye extracts from +/+, +/−, and −/− mice were separated on sodium dodecyl sulfate–12% poly acrylamide gel electrophoresis gels and transferred to a nitrocellulose mem-

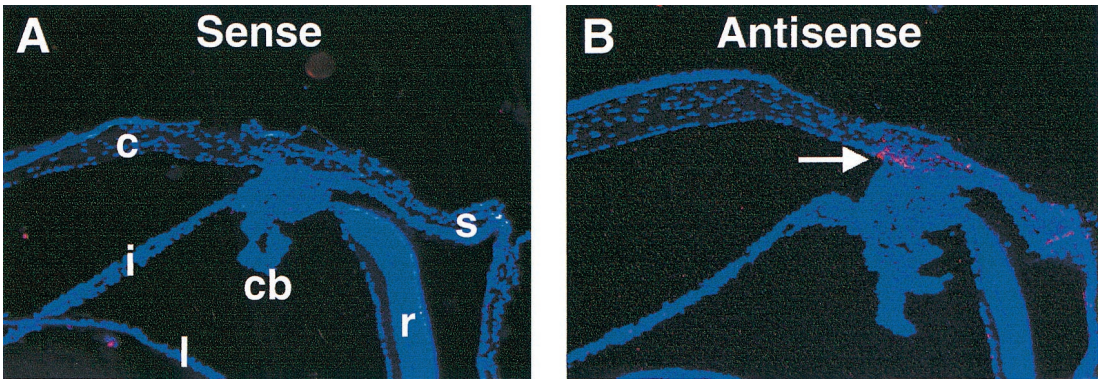

FIG. 2. Ocular expression of *Myoc*. High levels of *Myoc* mRNA expression are detected in the trabecular meshwork (B, arrow) located at the iridocorneal angle. cb, ciliary body; c, cornea; i, iris; l, lens; r, retina; s, sclera.

brane. After the membrane was blocked with Western blocking reagent (Boehringer Mannheim) and 5% skim milk in 0.05% Tween 20 and Tris-buffered saline (TBST) (pH 7.4) overnight at 4°C, it was incubated for 1 h with primary antibody in a 1:5,000 dilution made in TBST containing 1% skim milk. Anti-rabbit horseradish peroxidase-conjugated secondary antibody (Amersham) was used at a 1:2,500 dilution. The SuperSignal chemiluminescent detection system (Pierce) was used according to the manufacturer's instructions.

IOP measurement and clinical examination. F_1 mice were produced by mating chimeras derived from two independent lines, *TIGR7* and *TIGR8*, to strain B6 and were imported to the Jackson Laboratory. All of the mutant mice used in the IOP study retained the floxed *neomycin* (*neo*) cassette, and the age of the mice ranged from 3 to 16 months. Heterozygous B6/129 F_1 mice were backcrossed to B6 mice to produce +/+ and +/− N2 experimental mice. Heterozygous N2 mice were intercrossed to produce N2F1 experimental mice (+/+, +/−, and −/−). IOPs of the eyes of of male and female mice were measured as previously described (11, 12). IOP measurements of B6 mice are consistent over time, and so these animals were interspersed with experimental mice to ensure that calibration had not drifted and that the system was functioning optimally. Reported *P* values are from a multifactorial analysis of variance with genotype and sex as factors and age as a covariate.

Clinical anterior segment examinations were performed with a slit lamp biomicroscope. An indirect ophthalmoscope and a 60- or 90-diopter lens was used to visualize the retinas and optic nerves. For this analysis, pupils were dilated with a drop of 1% cyclopentolate. Fundus photographs were taken as previously reported (9). Clinical examinations were performed on male and female mice of each genotype at various ages, from 3 months and older. This included 12 $N2^{+/-}$ mice that were 10 to 15 months old and 25 $N2F1^{+/-}$ and $N2F1^{-/-}$ mice that were at least 10 months old.

Histological analysis. The preparation and analysis of thin plastic sections were performed essentially as described (26). Briefly, eyes were fixed in 4% paraformaldehyde in 0.1 M phosphate buffer (pH 7.2) for 2 h at room temperature. Eyes were then dehydrated in graded ethanol, oriented, and embedded in fresh Historesin (Leica, Heidelberg, Germany), following 8 days of infiltration. The embedded samples were dried and kept in a dehumidifying chamber (Dry Keeper; Sanplatec Corp., Osaka, Japan) until sectioning was performed. Semithin plastic sections were cut at 1.5-μm thicknesses using a microtome (RM 2165; Leica) and stained with hematoxylin and eosin.

EM. Electron microscopy (EM) procedures were performed essentially as described (26). Eyes were fixed for 1.5 h with 0.8% paraformaldehyde and 1.2% glutaraldehyde in 0.1 M phosphate buffer (pH 7.2) at 4°C. The anterior segment, which includes the cornea, iris, trabecular meshwork, and ciliary body, was cut into four equal-sized wedge-shaped blocks. These blocks were fixed further at 4°C for 12 h. Tissues were washed in PBS, postfixed with 1% osmium tetroxide, dehydrated in graded acetone, and embedded in Spurr's resin. Sections were cut and stained with uranyl acetate and lead citrate.

RESULTS

Expression of *Myoc* mRNA in the mouse eye. Ocular expression of *Myoc* was examined by RNA in situ hybridization. Eyes from newborn (postnatal day 0 [P0]) and 1-month-old +/+ mice on a mixed B6/129 genetic background were analyzed. At P0, no expression was detected (data not shown). At 1 month, strong expression was detected in the iridocorneal angle at the trabecular meshwork (Fig. 2). Our in situ experiments did not detect *Myoc* expression in ciliary body, iris, cornea, and retina, although other groups previously reported expression within these tissues (15, 33). The discrepancy between our findings and previously published data may be contributed to such factors as age differences between the animals.

Generation of *Myoc*-deficient mice. To elucidate the normal function of the gene product encoded by *Myoc*, we used homologous recombination in mouse ES cells to generate knockout mice lacking functional *Myoc*. Three independently targeted heterozygous ES cell clones were identified and injected into B6 blastocysts. Germ line transmission from each clone was obtained, and no subsequent differences were observed between different lines (Fig. 3A and B). To address the potential phenotypic variations that may be caused by genetic background effects, the mutant colony was expanded and maintained in both B6/129 mixed and 129 inbred genetic backgrounds. Additionally, the presence of exogenous sequences may also influence the activity of the targeted locus. To circumvent this potential problem, the mutant mice with the B6/129 background were also mated with B6 CMV-Cre (designating the mammalian cytomegalovirus minimal promoter fused to the Cre recombinase gene) mice for CRE-recombinase-mediated removal of the inserted *pgk-neomycin* cassette. The *Cre* transgene was then segregated from the *Myoc* mutants by crossing to B6. The occurrence of these events was verified by *neo*- and *Cre*-specific Southern strategies as described (4), and these mice were phenotypically indistinguishable from the mutant mice bearing the cassette (data not shown). To confirm the absence of normal MYOC protein in −/− mice, we used a polyclonal antibody directed against mouse MYOC to perform Western analysis. This antibody detected a single protein of approximately 55 kDa in +/+ and +/− eyes (Fig. 3C). The size of the protein closely matched the previously reported molecular weight of MYOC (15). This band was completely absent in eyes from −/− mice, while the intensity of band was reduced approximately twofold in +/− compared to +/+ mice. To address the possibility of residual transcript production from the targeted locus, RT-PCR was performed with poly$(A)^+$ RNA isolated from +/+, +/−, and −/− eyes at 1 month of age. Diagnostic 1.3- and 0.8-kb fragments were absent only from

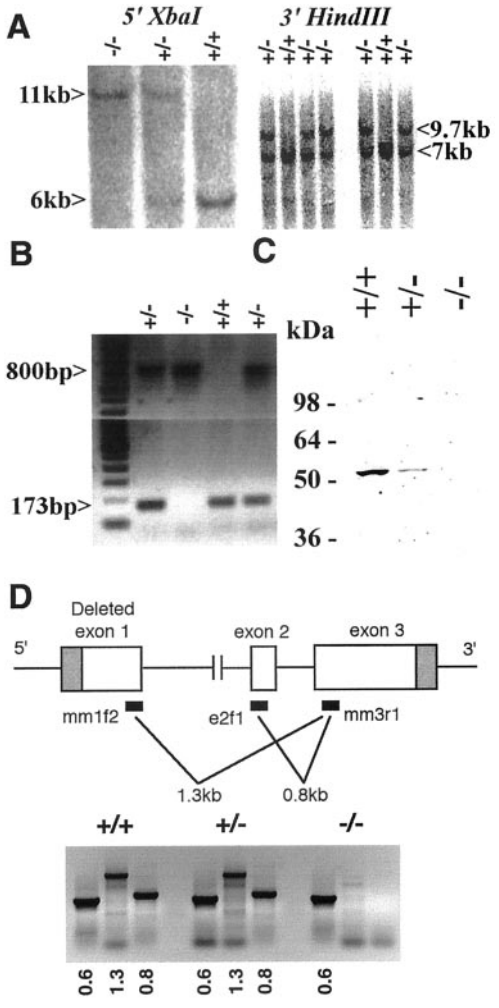

FIG. 3. Analysis of mutant mice deficient for *Myoc*. (A) Southern blot analysis of tail DNA. For both panels, upper bands correspond to the targeted alleles, while lower bands indicate the wild-type allele. Southern blot hybridization using the same sets of restriction enzymes and probes detected expected bands following *Cre*-mediated recombination (data not shown). (B) PCR genotype of tail DNA. An 800-bp fragment is specific for the *lacZ* cassette, which replaces the wild-type locus normally detected as a 173-bp fragment. (C) Western immunoblotting of eye homogenates. A polyclonal antibody against mouse MYOC was used. Protein extract was prepared from 1-month-old whole eye tissue. An approximately 55-kDa protein was detected in +/+ and +/− samples. No band was detected from the −/− sample. A faint band appearing at around 110 kDa in the +/+ sample may represent a trace amount of nonreduced MYOC dimer. (D) RT-PCR analysis of poly(A)$^+$ RNA collected from the eye. Fragments (1.3 or 0.8 kb) of *Myoc* were specifically absent in −/− mice, confirming the deletion of exon 1 and absence of residual transcript production from exon 2 and exon 3. A set of RT-PCR primers specific for mouse *Pax6* was used as a positive control and detected a 600-bp band from all three genotypes.

the −/− eyes, confirming the deletion of exon 1 and the absence of residual transcripts from exon 2 and exon 3 (Fig. 3D). For all RT-PCRs, any contamination from genomic DNA yields no product or a much larger product due to the presence of intron 1 and intron 2. RT-PCR for the inserted *lacZ* sequence detected 800-bp fragments from +/− and −/− eyes only (data not shown) with the same set of PCR primers used for genotyping as described earlier.

All mutant mice (+/− and −/−) were viable and fertile. Crosses of +/− breeding pairs resulted in +/+, +/−, and −/− progeny, roughly equal to the expected Mendelian ratio, indicating that neither +/− nor −/− genotype is lethal. Crosses between −/− mutant mice also produced litters in sizes similar to those of +/+ animals (data not shown), indicating that −/− mice are also fertile. Our results demonstrate that *Myoc* is not essential for the normal fertility and viability of the mouse.

IOP measurement and clinical examinations. To assess the effect of *Myoc* deficiency on IOP, we measured the IOPs of mice of each genotype at different ages. There was no significant difference in IOP between the genotypes (Fig. 4), suggesting that lack of *Myoc* does not lead to elevation of IOP. We also evaluated the anterior segment and fundus for clinical signs of glaucoma such as corneal edema, enlarged anterior chambers, and excavated or irregular optic nerves. All +/− and −/− eyes were normal compared to those of +/+ mice at all ages examined (data not shown).

Histological analysis. Our analysis focused on two regions of the eye, the anterior segment and the retina, including the optic nerve fibers. In the anterior segment, our analysis focused on the iridocorneal angle, which includes Schlemm's canal and the trabecular meshwork. The iridocorneal angle and outflow pathway of mice the eyes of mice similar to those of primates (26). Our histological examinations revealed no distinct abnormalities in +/− or −/− mice compared to age-matched +/+ mice ranging from 3 to 19 months old of age (+/+, $n = 6$ [B6/129 = 4, 129 = 2]; +/−, $n = 5$ [B6/129 = 3, 129 = 2]; −/−, $n = 8$ [B6/129 = 6, 129 = 2]). In all cases, both the Schlemm's canal and trabecular meshwork were present and the morphology of the iridocorneal angle was normal, including the ciliary body, which is the site of aqueous humor production. The cornea and iris also exhibited normal morphologies (Fig. 5A and B). The iridocorneal angle histology varied slightly between animals of the same genotype and between animals of different genotype. Nevertheless, these phenotypic variations were not consistently significant among or between the particular groups of animals. A similar phenotypic variation was observed even between the eyes from the same

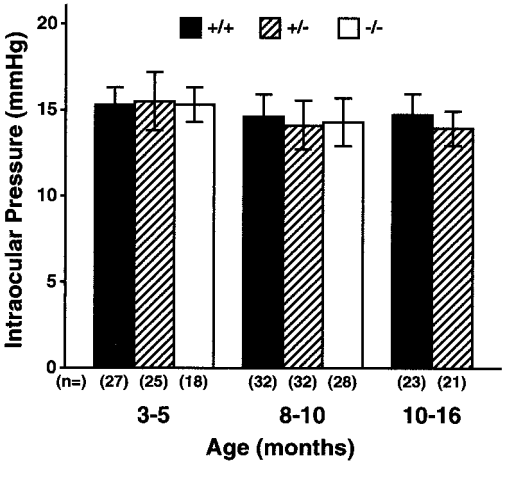

FIG. 4. Analysis of intraocular pressure (mean ± standard deviation). No significant difference in IOP was observed among the animals ranging from 3 to 16 months.

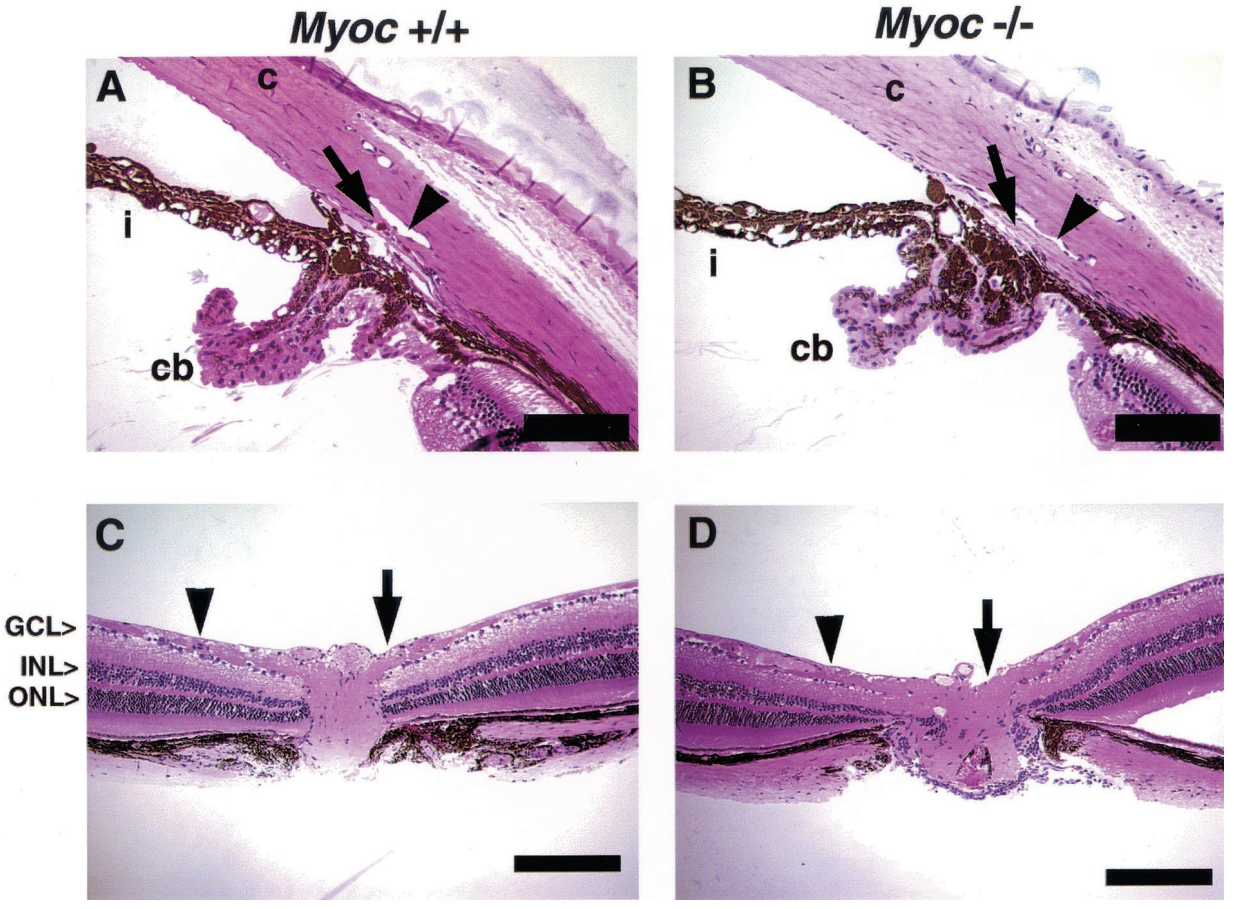

FIG. 5. Analysis of iridocorneal angle, retina, and optic nerve. Histological examinations revealed no distinct abnormalities of eyes collected from all three genotypes of age-matched animals. (A and B) Anterior segment. The Schlemm's canal (arrowhead), trabecular meshwork (arrow), cornea (c), iris (i), and ciliary body (cb) are well developed and appear to be normal in −/− tissue. The Schlemm's canal extends from a region above the posterior ciliary body to a region near the posterior cornea. An iris process attaches to the anterior trabecular meshwork in many cases. (C and D) The retina including optic nerve fibers and optic nerve head. The RGC layer (GCL) is approximately one to two cells thick, and the thickness and number of cells within the inner nuclear layer (INL) and outer nuclear layer (ONL) appear unchanged in −/− tissue. Nerve fibers (arrowheads) run laterally and converge at the optic nerve head (arrows), through which they exit the retina. The thickness of nerve fibers and the size of optic nerve head also appear normal in −/− eyes. All the histological examinations performed on age- and background-matched +/− mice also revealed no discernible phenotypes (data not shown). Scale bars: 100 μm (A and B) and 200 μm (C and D).

animal and within different sections from an individual eye. Besides the presence of normal, small variations in angle morphology, the overall ocular phenotype of mutant mice also matched closely with previously reported iridocorneal morphology of normal mice (26, 27).

Late-stage glaucoma displays a depletion of retinal ganglion cells (RGCs) and atrophy of optic nerve fibers as they enter the optic nerve head, resulting in cupping or excavation (6). We analyzed the retinas and optic nerve fibers of our mutant mice to detect these aberrations. +/− and −/− retinas had all of the retinal layers as +/+ retinas did. The number of cells within these layers appeared normal as did the overall thickness of the retina, including the optic nerve fiber layer and RGC layer (Fig. 5C and D). In agreement with the absence of IOP elevation, +/− and −/− mice had no apparent depletion of RGCs and displayed normal optic nerve fibers.

EM. We used transmission EM (TEM) to determine whether the targeted deletion of *Myoc* resulted in ultrastructural defects in specific ocular tissues. The trabecular meshwork, cornea, and iris were subjected to our TEM analysis. The trabecular meshwork provides major resistance to the outflow pathway. Consequently, the trabecular meshwork is believed to play a crucial role in regulating IOP and in the development of certain types of glaucoma (6, 25). For all the tissues examined, we again found no significant difference between +/+, +/−, and −/− eyes collected from 3-month-old to 1-year-old mice from both B6/129 and 129 genetic backgrounds. The results from +/+ and −/− littermates are shown (Fig. 6). The overall morphology of the iridocorneal angle and trabecular meshwork appeared normal in −/− mice, including the trabecular beams which surround drainage channels located in intertrabecular spaces. These trabecular beams also exhibited normal collagen fibers.

DISCUSSION

Evidence from human genetic studies indicates that dominantly inherited mutations in *MYOC* cause POAG. Affected

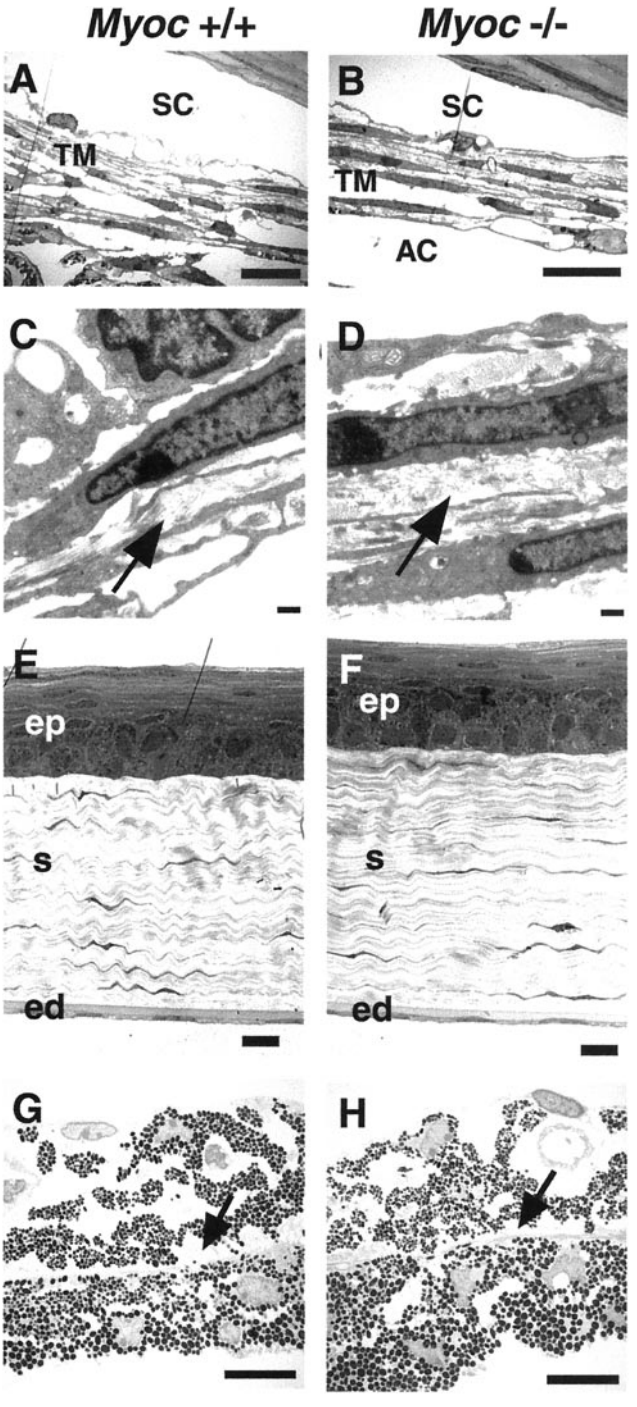

FIG. 6. TEM analyses of trabecular meshwork, cornea, and iris. −/− samples show no phenotypic differences that are consistently significant from +/+ samples. No difference was observed in corresponding tissues of +/− mice (data not shown). (A and B) The intertrabecular spaces and layered trabecular beams are present in the trabecular meshwork (TM), and Schlemm's canal (SC) has a normal morphology in both +/+ and −/− tissues. The posterior sections of the TM are shown in both panels A and B. The posterior TM generally contains more trabecular beams and extracellular matrix than the more anterior TM (data not shown; reference 26). A part of iris stroma is seen slightly attached to the uveal TM in +/+ tissue due to histological artifact, resulting in no obvious anterior chamber (AC) in the figure. (C and D) Higher magnification view of collagen fibers (arrow) within the trabecular beams. The collagen fibers are present and exhibit normal appearance in −/− tissue. (E and F) Corneal epithelium (ep), corneal stroma (s), and corneal endothelium (ed) appear unchanged in −/− tissue. (G and H) The iris shows no detectable differences in −/− tissue. The dilator muscle runs horizontally (arrow) dividing the iris stroma and iris epithelium. Scale bars: 10 μm (A, B, E, F, G, and H) and 500 nm (C and D).

individuals demonstrate a wide range of missense or nonsense mutations in their *MYOC* genes, with the vast majority of mutations localized to the terminal third exon. The mechanism of POAG formation in these individuals is unclear. One possibility is that individuals heterozygous for disease-causing mutations produce insufficient amounts of MYOC. Another possibility is that disease-causing mutations are gain of function, thus accounting for the dominant inheritance seen in *MYOC* pedigrees.

To address possible mechanisms for *MYOC*-induced glaucoma, we created a null mutation in the murine *Myoc* and assayed +/+, +/−, and −/− mice for alterations in ocular histopathology and IOP. Mice of each genotype were indistinguishable with respect to fertility, viability, IOP, trabecular meshwork histology and ultrastructure, and retinal and optic nerve morphology. Hence, we conclude that *Myoc* in mice is not required for either viability or for normal ocular morphology.

One possible reason for the lack of an observable phenotype in *Myoc*-null mutant mice is functional redundancy with other related gene products. *Myoc* shows homology to the olfactomedin gene, which encodes an extracellular matrix protein abundant in the nasal epithelium. Recently, an olfactomedin gene family was characterized in humans and designated *hOlfA* through *hOlfD* (17). These particular genes, however, do not contain the myosin-like domain found in *Myoc*, suggesting that *Myoc* is a unique member of the olfactomedin gene family. The isolation of genes containing both myosin- and olfactomedin-like domains will reinforce the possibility of functional redundancy. Functional studies and generation of double mutants with these genes will further test this possibility.

The lack of a discernable phenotype in both +/− and −/− mice also suggests that haploinsufficiency is not a critical mechanism for POAG in individuals with mutations in *MYOC*. Rather, disease-causing mutations are likely gain-of-function mutations. Of particular interest in this regard are recent studies that suggest that POAG is found only in patients with one wild-type copy and one mutant copy of *MYOC*. In a large French-Canadian family, Morissette and coworkers reported that glaucoma developed in three heterozygous siblings harboring missense mutations at codon 423 whereas four homozygous mutant siblings were asymptomatic for the disease (20). Since homozygous individuals do not manifest the disease, *MYOC*-associated mutation in these individuals cannot be classified as a conventional dominant-negative mutation. The authors suggest that heteromultimerization of mutant and wild-type forms of MYOC is a critical step in the pathogenesis of *MYOC*-induced glaucoma. These wild-type and mutant MYOC complexes could then lead to an accumulation of aberrant MYOC products in the cytoplasm or extracellular matrix, thereby impeding normal outflow of the aqueous humor. Additionally, the harmful accumulation of mutant MYOC may occur in RGCs or optic nerve fibers, undermining the structural integrity of these tissues and eventually lead to optic

neuropathies independent of elevation of IOP. The possibility of wild-type or mutant MYOC multimer formation interfering with the normal secretion of MYOC in vitro was also suggested by Jacobson and coworkers (10). Recently, Lam and coworkers reported the lack of a clinical phenotype in an elderly woman homozygous for the Arg46Stop mutation (18). This individual is believed to produce essentially no MYOC because the mutation would result in a prematurely truncated protein less than a tenth of the size of wild-type protein and with no putative functional domain. Our studies demonstrating that reduction or lack of MYOC in mice does not lead to POAG are consistent with these models for the pathogenesis of *MYOC*-associated POAG. Further studies, including the generation and characterization of mice with point mutations in exon 3 of *Myoc*, should aid in determining the precise mechanisms leading to *MYOC*-associated POAG.

ACKNOWLEDGMENTS

We thank Kenneth Dunner and the M. D. Anderson Cancer Center Electron Microscope Core facility for TEM analysis, Adriana Zabaleta for technical advice and assistance, and Dr. Richard Behringer for helpful comments on the manuscript. B.S.K. thanks former colleagues at Alkermes, Inc., for encouragement.

This work was supported in part by M. D. Anderson Cancer Center Core Grants to the veterinary services and Electron Microscope and DNA Sequencing core facilities, an NIH predoctoral training grant (EY0702420) to B.S.K., an NIH postdoctoral training grant (5F32EY06945) to M.V.R., and an NIH grant (EY123113) to R.L.J. S.W.M.J. is an Assistant Investigator of the Howard Hughes Medical Institute.

REFERENCES

1. **Abderrahim, H., V. L. Jaramillo-Babb, Z. Zhou, and D. Vollrath.** 1998. Characterization of the murine TIGR/myocilin gene. Mamm. Genome **9:**673–675.
2. **Adam, M. F., A. Belmouden, P. Binisti, A. P. Brezin, F. Valtot, A. Bechetoille, J. C. Dascotte, B. Copin, L. Gomez, A. Chaventre, J. F. Bach, and H. J. Garchon.** 1997. Recurrent mutations in a single exon encoding the evolutionarily conserved olfactomedin-homology domain of TIGR in familial open-angle glaucoma. Hum. Mol. Genet. **6:**2091–2097.
3. **Albrecht, U., R. Abu-Issa, B. Ratz, M. Hattori, J. Aoki, H. Arai, K. Inoue, and G. Eichele.** 1996. Platelet-activating factor acetylhydrolase expression and activity suggest a link between neuronal migration and platelet-activating factor. Dev. Biol. **180:**579–593.
4. **Arango, N. A., R. Lovell-Badge, and R. R. Behringer.** 1999. Targeted mutagenesis of the endogenous mouse Mis gene promoter: in vivo definition of genetic pathways of vertebrate sexual development. Cell **99:**409–419.
5. **Chen, H., Y. Lun, D. Ovchinnikov, H. Kokubo, K. C. Oberg, C. V. Pepicelli, L. Gan, B. Lee, and R. L. Johnson.** 1998. Limb and kidney defects in Lmx1b mutant mice suggest an involvement of LMX1B in human nail patella syndrome. Nat. Genet. **19:**51–55.
6. **Choplin, N. T., and D. C. Lundy.** 1998. Atlas of glaucoma. Martin Dunitz Ltd., London, England.
7. **Gage, P. J., and S. A. Camper.** 1997. Pituitary homeobox 2, a novel member of the bicoid-related family of homeobox genes, is a potential regulator of anterior structure formation. Hum. Mol. Genet. **6:**457–464.
8. **Hanson, I. M., J. M. Fletcher, T. Jordan, A. Brown, D. Taylor, R. J. Adams, H. H. Punnett, and V. van Heyningen.** 1994. Mutations at the PAX6 locus are found in heterogeneous anterior segment malformations including Peters' anomaly. Nat. Genet. **6:**168–173.
9. **Hawes, N. L., R. S. Smith, B. Chang, M. Davisson, J. R. Heckenlively, and S. W. John.** 1999. Mouse fundus photography and angiography: a catalogue of normal and mutant phenotypes. Mol. Vis. **5:**22.
10. **Jacobson, N., M. Andrews, A. R. Shepard, D. Nishimura, C. Searby, J. H. Fingert, G. Hageman, R. Mullins, B. L. Davidson, Y. H. Kwon, W. L. Alward, E. M. Stone, A. F. Clark, and V. C. Sheffield.** 2001. Non-secretion of mutant proteins of the glaucoma gene myocilin in cultured trabecular meshwork cells and in aqueous humor. Hum. Mol. Genet. **10:**117–125.
11. **John, S. W., J. R. Hagaman, T. E. MacTaggart, L. Peng, and O. Smithes.** 1997. Intraocular pressure in inbred mouse strains. Investig. Ophthalmol. Vis. Sci. **38:**249–253.
12. **John, S. W., R. S. Smith, O. V. Savinova, N. L. Hawes, B. Chang, D. Turnbull, M. Davisson, T. H. Roderick, and J. R. Heckenlively.** 1998. Essential iris atrophy, pigment dispersion, and glaucoma in DBA/2J mice. Investig. Ophthalmol. Vis. Sci. **39:**951–962.
13. **Karali, A., P. Russell, F. H. Stefani, and E. R. Tamm.** 2000. Localization of myocilin/trabecular meshwork—inducible glucocorticoid response protein in the human eye. Investig. Ophthalmol. Vis. Sci. **41:**729–740.
14. **Kidson, S. H., T. Kume, K. Deng, V. Winfrey, and B. L. Hogan.** 1999. The forkhead/winged-helix gene, Mf1, is necessary for the normal development of the cornea and formation of the anterior chamber in the mouse eye. Dev. Biol. **211:**306–322.
15. **Kubota, R., S. Noda, Y. Wang, S. Minoshima, S. Asakawa, J. Kudoh, Y. Mashima, Y. Oguchi, and N. Shimizu.** 1997. A novel myosin-like protein (myocilin) expressed in the connecting cilium of the photoreceptor: molecular cloning, tissue expression, and chromosomal mapping. Genomics **41:**360–369.
16. **Kulak, S. C., K. Kozlowski, E. V. Semina, W. G. Pearce, and M. A. Walter.** 1998. Mutation in the RIEG1 gene in patients with iridogoniodysgenesis syndrome. Hum. Mol. Genet. **7:**1113–1117.
17. **Kulkarni, N. H., C. A. Karavanich, W. R. Atchley, and R. R. Anholt.** 2000. Characterization and differential expression of a human gene family of olfactomedin-related proteins. Genet. Res. **76:**41–50.
18. **Lam, D. S., Y. F. Leung, J. K. Chua, L. Baum, D. S. Fan, K. W. Choy, and C. P. Pang.** 2000. Truncations in the TIGR gene in individuals with and without primary open-angle glaucoma. Investig. Ophthalmol. Vis. Sci. **41:**1386–1391.
19. **Lutjen-Drecoll, E.** 1999. Functional morphology of the trabecular meshwork in primate eyes. Prog. Retin. Eye Res. **18:**91–119.
20. **Morissette, J., C. Clepet, S. Moisan, S. Dubois, E. Winstall, D. Vermeeren, T. D. Nguyen, J. R. Polansky, G. Cote, J. L. Anctil, M. Amyot, M. Plante, P. Falardeau, and V. Raymond.** 1998. Homozygotes carrying an autosomal dominant TIGR mutation do not manifest glaucoma. Nat. Genet. **19:**319–321.
21. **Nguyen, T. D., P. Chen, W. D. Huang, H. Chen, D. Johnson, and J. R. Polansky.** 1998. Gene structure and properties of TIGR, an olfactomedin-related glycoprotein cloned from glucocorticoid-induced trabecular meshwork cells. J. Biol. Chem. **273:**6341–6350.
22. **Nishimura, D. Y., R. E. Swiderski, W. L. Alward, C. C. Searby, S. R. Patil, S. R. Bennet, A. B. Kanis, J. M. Gastier, E. M. Stone, and V. C. Sheffield.** 1998. The forkhead transcription factor gene FKHL7 is responsible for glaucoma phenotypes which map to 6p25. Nat. Genet. **19:**140–147.
23. **Polansky, J. R., D. J. Fauss, P. Chen, H. Chen, E. Lutjen-Drecoll, D. Johnson, R. M. Kurtz, Z. D. Ma, E. Bloom, and T. D. Nguyen.** 1997. Cellular pharmacology and molecular biology of the trabecular meshwork inducible glucocorticoid response gene product. Ophthalmologica **211:**126–139.
24. **Quigley, H. A., and S. Vitale.** 1997. Models of open-angle glaucoma prevalence and incidence in the United States. Investig. Ophthalmol. Vis. Sci. **38:**83–91.
25. **Shields, M. B.** 1997. Textbook of glaucoma, 4th ed. Lippincott, Williams & Wilkins, Baltimore, Md.
26. **Smith, R. S., A. Zabaleta, T. Kume, O. V. Savinova, S. H. Kidson, J. E. Martin, D. Y. Nishimura, W. L. Alward, B. L. Hogan, and S. W. John.** 2000. Haploinsufficiency of the transcription factors FOXC1 and FOXC2 results in aberrant ocular development. Hum. Mol. Genet. **9:**1021–1032.
27. **Smith, R. S., A. Zabaleta, O. V. Savinova, and S. W. John.** 2001. The mouse anterior chamber angle and trabecular meshwork develop without cell death. BMC Dev. Biol. **1:**3.
28. **Stoilova, D., A. Child, G. Brice, R. P. Crick, B. W. Fleck, and M. Sarfarazi.** 1997. Identification of a new 'TIGR' mutation in a family with juvenile-onset primary open angle glaucoma. Ophthalmic Genet. **18:**109–118.
29. **Stoilova, D., A. Child, G. Brice, T. Desai, M. Barsoum-Homsy, N. Ozdemir, L. Chevrette, M. F. Adam, H. J. Garchon, R. Pitts Crick, and M. Sarfarazi.** 1998. Novel TIGR/MYOC mutations in families with juvenile onset primary open angle glaucoma. J. Med. Genet. **35:**989–992.
30. **Stone, E. M., J. H. Fingert, W. L. M. Alward, T. D. Nguyen, J. R. Polansky, S. L. F. Sunden, D. Nishimura, A. F. Clark, A. Nystuen, B. E. Nichols, D. A. Mackey, R. Ritch, J. W. Kalenak, E. R. Craven, and V. C. Sheffield.** 1997. Identification of a gene that causes primary open angle glaucoma. Science **275:**668–670.
31. **Suzuki, Y., S. Shirato, F. Taniguchi, K. Ohara, K. Nishimaki, and S. Ohta.** 1997. Mutations in the TIGR gene in familial primary open-angle glaucoma in Japan. Am. J. Hum. Genet. **61:**1202–1204.
32. **Swiderski, R. E., L. Ying, M. D. Cassell, W. L. Alward, E. M. Stone, and V. C. Sheffield.** 1999. Expression pattern and in situ localization of the mouse homologue of the human MYOC (GLC1A) gene in adult brain. Brain Res. Mol. Brain Res. **68:**64–72.
33. **Takahashi, H., S. Noda, Y. Imamura, A. Nagasawa, R. Kubota, Y. Mashima, J. Kudoh, Y. Oguchi, and N. Shimizu.** 1998. Mouse myocilin (Myoc) gene expression in ocular tissues. Biochem. Biophys. Res. Commun. **248:**104–109.
34. **Tomarev, S. I., E. R. Tamm, and B. Chang.** 1998. Characterization of the mouse Myoc/Tigr gene. Biochem. Biophys. Res. Commun. **245:**887–893.
35. **Vollrath, D., V. L. Jaramillo-Babb, M. V. Clough, I. McIntosh, K. M. Scott, P. R. Lichter, and J. E. Richards.** 1998. Loss-of-function mutations in the LIM-homeodomain gene, LMX1B, in nail-patella syndrome. Hum. Mol. Genet. **7:**1091–1098.
36. **Yokoe, H., and R. R. Anholt.** 1993. Molecular cloning of olfactomedin, an extracellular matrix protein specific to olfactory neuroepithelium. Proc. Natl. Acad. Sci. USA **90:**4655–4659.